The Company of Biologists

Investigating the morphological dynamics of the plasma membrane by high-speed atomic force microscopy

Yiming Yu and Shige H. Yoshimura*

ABSTRACT

Despite numerous recent developments in bioimaging techniques, nanoscale and live-cell imaging of the plasma membrane has been challenging because of the insufficient z-resolution of optical microscopes, as well as the lack of fluorescent probes to specifically label small membrane structures. High-speed atomic force microscopy (HS-AFM) is a powerful tool for visualising the dynamics of a specimen surface and is therefore suitable for observing plasma membrane dynamics. Recent developments in HS-AFM for live-cell imaging have enabled the visualisation of the plasma membrane and the network of cortical actin underneath the membrane in a living cell. Furthermore, correlative imaging with fluorescence microscopy allows for the direct visualisation of morphological changes of the plasma membrane together with the dynamic assembly or disassembly of proteins during the entire course of endocytosis in a living cell. Here, we review these recent advances in HS-AFM in order to analyse various cellular events occurring at the cell surface.

KEY WORDS: High-speed atomic force microscopy, Live-cell imaging, Clathrin-mediated endocytosis, Cortical actin

Introduction

The plasma membrane separates the intracellular space from the extracellular environment and prevents the free passage of molecules between the two spaces. It also functions as an important hub for the transducing of cellular information by a large variety of membrane proteins, such as receptors and channels, as well as through dynamic morphological changes of the membrane, such as endocytosis and exocytosis. Various endocytic pathways, such as clathrin-mediated endocytosis (CME), caveolae-mediated trafficking and pinocytosis, facilitate the incorporation of extracellular molecules into the cytoplasm, while exocytosis and exosomes release intracellular molecules into the extracellular space. A global understanding of such a complex web of information networks requires elucidating individual mechanisms of how distinct sets of proteins coordinate a series of membrane-reshaping processes. Recent advancements in fluorescence imaging techniques (fluorescent probes and microscopic observation techniques) have revealed the spatiotemporal dynamics of individual proteins involved in these processes (Arasada et al., 2018; McMahon and Boucrot, 2011; Taylor et al., 2011; Weinberg and Drubin, 2012). By contrast, morphological analyses of the plasma membrane during these processes largely relied on electron microscopy (EM), which yields high-resolution images of small

membrane architectures, such as clathrin-coated vesicles (CCVs) (Higgins and McMahon, 2002; Royle and Lagnado, 2003). Despite these imaging techniques, following the morphological dynamics of the plasma membrane during endocytosis has been a difficult task because of the lack of a labelling method for the membrane.

Atomic force microscopy (AFM), which was originally developed to visualise the surface topography of metal specimens, has been used to visualise biomolecules, such as proteins, chromatin, nuclear pores and biomembranes (Binnig et al., 1986; Edstrom et al., 1990; Leuba et al., 1994; Oberleithner et al., 1995; Wang and Clapham, 1999; Weisenhorn et al., 1990). One of the biggest advantages of AFM in biology is that it can obtain topographic information of biomolecules at nanometre resolution without fixation, staining or labelling of the specimen, which is generally required for the optical microscopy and electron microscopy. In AFM, the surface of a specimen is scanned with a sharp probe (typically made of silicon or silicon nitride) attached to one end of a long cantilever (∼100 μm length). Therefore, the spatial and temporal resolutions of AFM imaging depend on the sharpness of the probe and the scanning speed, respectively. In more than 20 years of AFM history in biology, various technical developments have been made to improve spatiotemporal resolution (Akita et al., 1999; Ando et al., 2001). In particular, the development of high-speed AFM (HS-AFM) has made enormous contributions to visualising the structural dynamics of biomolecules and cellular structures.

To date, HS-AFM has been used to explore DNA nanostructures (Endo et al., 2012; Sannohe et al., 2010), conformational changes in proteins (Casuso et al., 2012; Kodera et al., 2010; Yokokawa et al., 2006), enzyme activity (Igarashi et al., 2011; Uchihashi et al., 2011), and protein–nucleic acid interactions (Gilmore et al., 2009; Sanchez et al., 2011; Suzuki et al., 2011). However, despite its high spatiotemporal resolution, the application of HS-AFM to living cells has been challenging and requires overcoming technical limitations, such as broadening of the scanning area, precise positioning of cantilevers and avoidance of potential damage to the cell surface caused by the probe. Here, we review the technical advances in HS-AFM for live-cell imaging and highlight how it has been utilised to understand the morphological and molecular dynamics of a living cell surface.

Principles of AFM imaging

In AFM, a scanning-probe microscope with a sharp probe is used to visualise the surface of the specimen. Most AFM setups use a probe (a few nanometres in tip radius) attached to the end of a flat cantilever to obtain topographical information with sub-nanometre resolution. The deflection of the cantilever during scanning is amplified by a mechanism called 'light lever', in which a laser beam is spotted on the back of the cantilever, and the angle of the reflected beam is detected by a position-sensitive detector placed far from the cantilever (Hansma et al., 1988). There are three major operating modes in AFM: contact, tapping and non-contact (Box 1). Although the

Graduate School of Biostudies, Kyoto University, Yoshida-konoe, Sakyo-ku, Kyoto 606-8501, Japan.

*Author for correspondence (yoshimura@lif.kyoto-u.ac.jp)

Y.Y., 0000-0001-7193-9080; S.H.Y., 0000-0001-6033-1301

Box 1. Operating principles of AFM

AFM visualises the morphology of a specimen by using a sharp probe that is attached to the end of a thin and flat cantilever. The deflection of the cantilever induced by direct and indirect contact with the specimen surface is detected by an optical system called the 'light-lever', in which a laser beam spot is focused on the back of the cantilever and the reflected light is captured by a position-sensitive detector placed in a distance. During scanning, the signal from the position-sensitive detector is fed back to the piezo scanner that drives the stage to move in the z-direction to keep the deflection value the same as a reference value (setpoint). Meanwhile, the cantilever moves in the x-y direction so that a two-dimensional map of height (z) information can be obtained. Three major scanning modes are available: contact, tapping and non-contact (see figure). In the contact mode, the probe directly contacts and scans along the specimen surface and the deflection of the cantilever is used for feedback control (Binnig et al., 1986). In the tapping mode, the cantilever is vibrated near its resonance frequency by using a piezo, which is mounted on a cantilever holder (Zhong et al., 1993). The amplitude of the cantilever is monitored by the detector and used for the feedback control; it keeps the amplitude constant by moving the stage in the z-direction. As the damage to the specimen is much smaller than in the contact mode, this mode is most widely used in bio-imaging, including HS-AFM (Giessibl, 2003). In the non-contact mode, the cantilever oscillates at its resonance frequency but does not physically contact the specimen surface (Martin et al., 1987). When the tip of the probe gets close to the specimen surface, the amplitude or phase of the cantilever is affected by a long-range force (such as Van der Waals) between the probe and the surface. The feedback system uses either amplitude or phase to control the stage. Although the non-contact mode does not damage the specimen, it has a low spatial resolution compared to the other two modes and is not frequently used in bio-imaging (Giessibl, 2003).
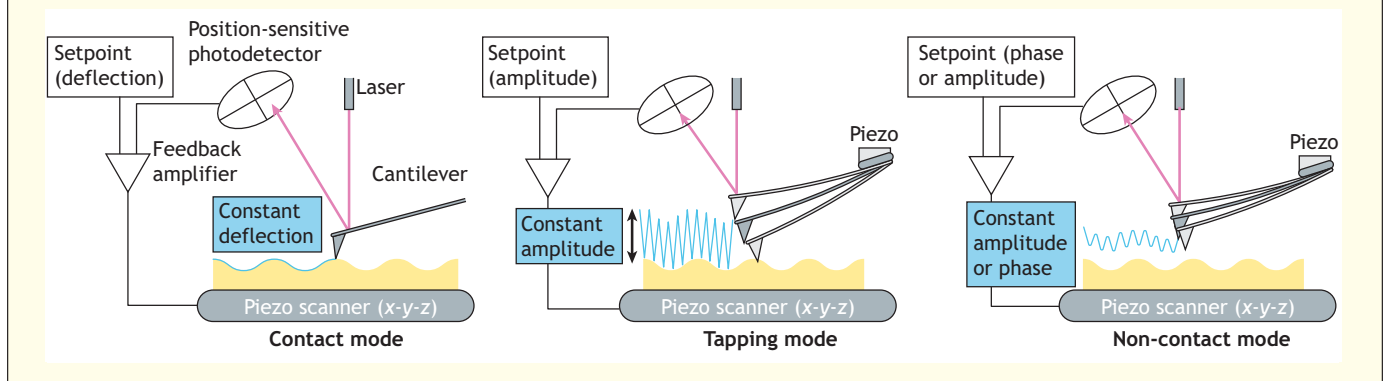
contact mode is the fastest and most sensitive, it is not suitable for biomolecules because the hard probe damages the specimen during scanning. The tapping mode is most widely used in bio-imaging owing to its relatively high resolution and small damage. The disadvantages of the tapping mode are the mechanical requirement for vibrating the cantilever (at its resonance frequency), and the effect of the cantilever vibration on the sample, especially when imaging the sample in liquid (Putman et al., 1994).

One of the biggest advantages of AFM is that it visualises the shape of biomolecules in liquid at nanometre resolution without fixation, staining or labelling. This is in clear contrast to electron microscopy, which requires fixation and staining of the sample and a vacuum environment for imaging. Fluorescence-based imaging techniques also contrast with AFM in this regard, as the molecule of interest needs to be labelled either by a specific fluorescent dye or by fusion with a fluorescent protein. Fluorescence microscopy provides the 'location' of the molecule of interest, whereas AFM provides the shape of the molecule. Although the spatial resolution of fluorescence microscopy has been greatly improved by the development of super-resolution microscopy, AFM remains distinct from any of the fluorescence-based techniques because it provides different types of structural information. As described in later sections, AFM and fluorescence microscopy are complementary to each other, and can be combined to enable correlative imaging. As both techniques can now handle living cells, live-cell correlative imaging is one of the most powerful imaging techniques in cell biology.

Temporal resolution has also been an important subject for the broader application of AFM in biology. In the early stage of AFM development, the frame rate ranged from being greater than a few seconds to tens of seconds (Giessibl, 2003); therefore, molecular

events that occurred at a faster pace than the frame speed had to be slowed down by either reducing the substrate concentration, decreasing the temperature, or interfering with the substrate surface (Guthold et al., 1999; Kasas et al., 1997). Shortcomings in the scanning speed led to the design of AFM devices with high-speed scanning units. One early development in fast-scanning AFM involved using a cantilever with a low resonant frequency and large spring constant, which could easily damage biological samples (Minne et al., 1998; Sulchek et al., 1999). The situation was improved by the development of a small cantilever (~2 μm in width, ~10 μm in length), which resulted in a lower force (less than ~10 pN in the case of HS-AFM, and several tens to hundreds of pN in conventional AFMs) and reduced damage to the specimen (Ando et al., 2001; Viani et al., 1999; Walters et al., 1996).

In addition to the small cantilevers, a fast and stable scanner and its control systems for HS-AFM were developed in 2008 (Ando et al., 2008). This HS-AFM system achieved a video-rate time resolution (30 frames/s) with nanometre spatial resolution, and helped visualise a number of molecular events and structural dynamics of biomolecules in the order of milliseconds (Ando, 2018; Uchihashi et al., 2016). In recent years, the application of HS-AFM has been directed toward the molecular dynamics in living cells, which will be described in the following section.

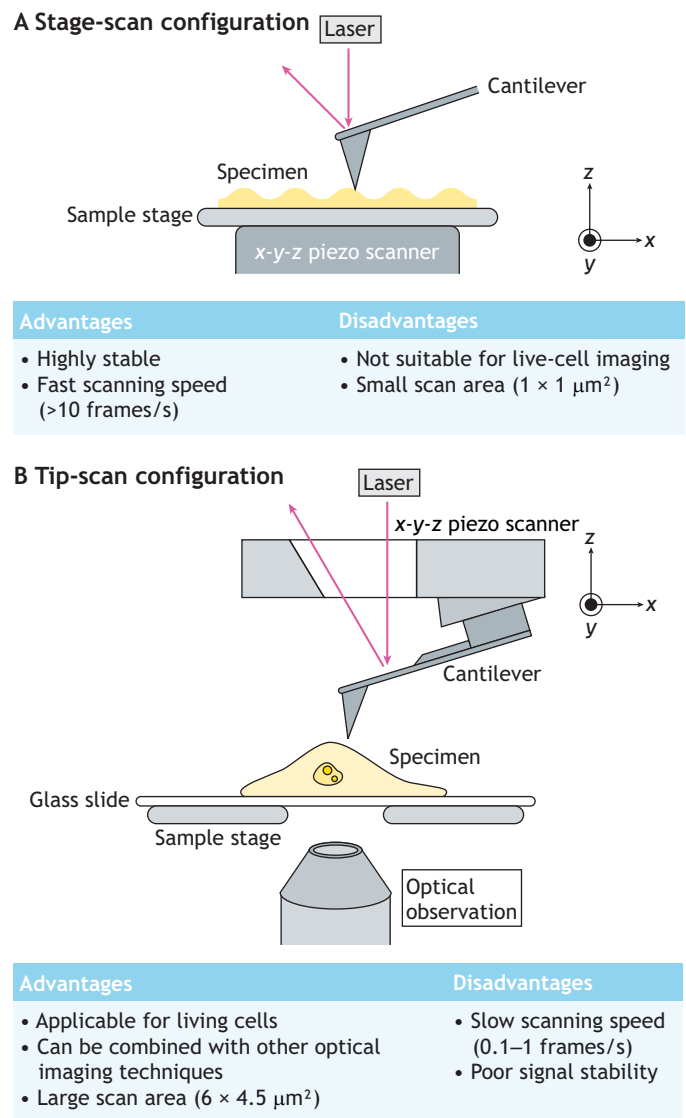## Development of HS-AFM for live-cell imaging

Because the AFM probe directly 'touches' the specimen surface, the resolution more-or-less depends on the strength of the touch; touching with a larger force enables more detailed structural information than that with a soft touch. This is similar to the situation in which one attempts to recognise the shape of an object

without seeing it and only using hands; when you touch the object hard, you can recognise it in more detail. This is true for biomolecules such as DNA that are directly attached to solid surfaces like glass or mica. However, the situation becomes completely different when one attempts to observe the molecular action on the surface of a living cell. Cultured animal cells are much softer and more fragile than a probe, even when they are grown on a solid substrate (e.g. glass); this is similar to a piece of jelly on a flat plate. Imaging the nanostructures on a living cell surface by AFM is similar to touching a piece of jelly on a plate with a hard needle; applying a strong force does not increase the spatial resolution, but rather deforms the specimen. Therefore, imaging the plasma membrane is a challenge that must resolve two incompatible issues, minimising the deformation of the soft specimen and achieving high spatial resolution.

In addition, the following issues need to be addressed for the efficient imaging of the surface structures of the plasma membrane. First, using an AFM system in combination with an optical microscope is necessary for positioning the cantilever in the area of interest. Although this method has been widely used in many conventional AFM devices, it is difficult in HS-AFM because this method requires a 'tip-scan' (and not a 'stage-scan') configuration (see below). Second, a large scanning area of several micrometres is required owing to the density and frequency of endocytic events [0.04 ± 0.01 pits/μm^2 min; Yoshida et al., 2018]. Many HS-AFM devices typically have a scanning area of ~1 μm^2. This means that one can observe endocytosis only a few times in an hour, which is unrealistic. Broadening the scanning area is not a simple task because of the trade-off between the scanning area and temporal resolution; to achieve a large scanning area with a constant velocity of the cantilever, the temporal resolution has to be sacrificed. We describe these two issues in the following sections.

Two typical scanning configurations that are widely used in current HS-AFM systems are summarised in Fig. 1. In the 'stage-scan' configuration (Fig. 1A), the specimen is placed on a piezo scanner which moves in the x-y-z directions. The position of the cantilever with a light-lever system is fixed. During the imaging, the cantilever vibrates at a fixed position and the stage moves in the x, y and z directions. This configuration can achieve a high level of mechanical stability during high-speed scanning (over 10 frames per second) (Ando et al., 2001), and has been utilised in live-cell imaging of bacterial cells to reveal the dynamic behaviour of nano-machineries on the bacterial cell surface (Kobayashi et al., 2021; Yamashita et al., 2012). However, it is not suitable for combination with an optical microscope because the sample stage is not transparent. In contrast, the 'tip-scan' configuration (Fig. 1B) has a cantilever with a light-lever system, which moves in the x, y and z directions using a piezo scanner. This all-in-one scanning system is mounted on the stage of an inverted microscope so that it can image the specimen, such as a living cell placed on the stage. This enables correlative imaging using HS-AFM and fluorescence microscopy, which is a powerful imaging system as it provides information on both the localisation of a protein of interest and the morphological changes in the related cellular structures. A disadvantage of the tip-scan configuration is its complex all-in-one optical system; the laser spot needs to follow the scanning cantilever, which reduces the signal stability rapidly as the scanning speed increases (Suzuki et al., 2013).

The scanning area of live-cell HS-AFM has also been improved. Many HS-AFM devices designed for single-molecule imaging have a 'stage-scan' configuration and a scanning area of less than 1×1 μm^2 (Ando et al., 2001). This is suitable for stable high-speed scanning of biological molecules, such as proteins and nucleic acids or frequently

A Stage-scan configuration

Advantages	Disadvantages
• Highly stable • Fast scanning speed (>10 frames/s)	• Not suitable for live-cell imaging • Small scan area (1 × 1 μm^2)

B Tip-scan configuration

Advantages	Disadvantages
• Applicable for living cells • Can be combined with other optical imaging techniques • Large scan area (6 × 4.5 μm^2)	• Slow scanning speed (0.1–1 frames/s) • Poor signal stability

Fig. 1. Stage-scan and tip-scan configurations of HS-AFM. Schematic illustrations of currently available stage-scan (A) and tip-scan (B) configurations of HS-AFM. (A) In the stage-scan configuration, the specimen is set on a stage on an x-y-z piezo scanner. The x-y position of the cantilever probe is fixed, and it vibrates to tap the specimen surface. This enables a stable light-lever system of the cantilever and fast scanning of the stage at the same time. However, as the stage on the piezo scanner is not transparent, the specimen cannot be observed by an optical microscope system. (B) In the tip-scan configuration, the specimen is placed on the stage of an inverted microscope. A cantilever is controlled by an x-y-z piezo scanner mounted on the stage and scans the specimen surface. This configuration enables optical observation of the specimen (e.g. a living cell) on the stage from the bottom and its AFM observation from above. As the light-lever system has to move together with the scanning cantilever, the fast-scanning operation is more difficult.

observed cellular structures such as synaptic vesicles (~200 vesicles/ μm^2; Zhang et al., 1998); however, such an area is too small to efficiently capture rare cellular events on the cell surface, such as endocytosis, as we mentioned in the previous section. Because the scanning area and scanning rate are a trade-off as noted above, live-cell HS-AFM devices are equipped with a larger scanner with some sacrifice of the scanning rate. For instance, a stage-scan type HS-AFM equipped with a scanner with a scanning area of ~46×46 μm^2 has successfully captured a bacteriolysis process of *B. subtilis*

(20×20 μm² at 5 s per frame) and endocytosis on the surface of HeLa cells (5×5 μm² at 5 s per frame) (Watanabe et al., 2013). The scanning area of the tip-scan HS-AFM set-up was also improved and enabled the scanning of an area of ∼3.5×4.5 μm² every 10 s (Suzuki et al., 2013). More recently, we were able to expand the scanning area of the tip-scan HS-AFM device to 4.5×6.0 μm², which allowed us to visualise various endocytic structures, including clathrin-coated pits (CCPs) and caveolae (Yoshida et al., 2018).

Impact of live-cell HS-AFM on endocytosis research

Different endocytic pathways are mediated by different proteins. Small membrane invaginations are mediated by coat proteins, such as clathrin in the case of CME and caveolin for caveolae; however, several other endocytic pathways that do not involve coated structures have been characterised, such as macropinocytosis, phagocytosis and endocytosis mediated by other clathrin-independent carriers (CLICs) (Flannagan et al., 2012; Howes et al., 2010; Swanson and Watts, 1995). In addition, the glycosylphosphotidylinositol-anchored protein (GPI-AP)-enriched early endosomal compartment (GEEC), a tubulation of the plasma membrane mediated by CLICs, has also been described (Sabharanjak et al., 2002). Some of these pathways include a unique 'marker' protein, which can distinguish a pathway or a structure (e.g. clathrin for CME and caveolin for caveolae), while others share factors, such as dynamin and actin. The entire process of CME involves more than 30 different proteins, which induce a series of morphological changes in the plasma membrane (Kaksonen and Roux, 2018; McMahon and Boucrot, 2011).

The biggest advantage of live-cell HS-AFM to research endocytosis is that it can visualise the morphological changes in the plasma membrane of a living cell. Although many fluorescence-based imaging techniques have revealed the spatiotemporal assembly of related proteins in the CCP (Arasada et al., 2018; Fujimoto et al., 2000; Grassart et al., 2014; Shimada et al., 2007), they do not provide information on the 'shape' of the membrane. Therefore, the use of correlative imaging using fluorescence microscopy and HS-AFM has had a significant effect on this field. The following are some examples of successful application of correlative imaging to CME.

Mechanism of CME revealed by live-cell correlative imaging using HS-AFM

The moment when the CCP is completely closed has been difficult to determine from the fluorescence signal of clathrin because the clathrin coat remains on the vesicle after scission from the plasma membrane. The moment of CCP closing has been determined by labelling CCPs with pH-sensitive fluorescent proteins (transferrin receptor fused with phluorin) and rapidly exchanging the pH of the external medium between 7.4 and 5.5, which turns the fluorescence on and off (Merrifield et al., 2005). In contrast, live-cell HS-AFM has allowed the visualisation of the entire process of CME, from the initial membrane invagination to the complete closure of the pit (Yoshida et al., 2018). Furthermore, correlative imaging with confocal laser-scanning microscopy (CLSM) has been able to reveal the spatiotemporal correlation between protein assembly and pit closing; in COS7 cells, the CCP closed ∼2 s after the peak of dynamin (the moment when the fluorescence intensity of dynamin reaches the maximum value) and at ∼3 s before the clathrin signal disappeared (Yoshida et al., 2018). Similarly, the existence of a so-called 'hot spot', where a CCP is successively generated at the same position (Nunez et al., 2011; Saffarian et al., 2009), has also been probed with live-cell HS-AFM (Yoshida et al., 2018) (see the next

section for details). In addition to providing insights into the closing step, HS-AFM has been used to correlate the initiation of membrane invagination with the assembly of epsin (Yoshida et al., 2018), which is known to be associated with clathrin to promote membrane bending in the early stages of CME (Chen et al., 1998).

Another new insight concerns the process by which polymerisation of clathrin curves the plasma membrane into a spherical pit. Two models have been proposed based on EM images – the 'constant radius' model, in which the diameter of the CCP remains the same with the growth of the clathrin-coated area, and the 'constant area' model in which the clathrin lattice remains flat until the coated area reaches a certain size, with the membrane then gradually invaginating into a spherical shape (Kaksonen and Roux, 2018). Correlative live-cell HS-AFM and CLSM imaging revealed a good correlation between the amount of clathrin and invagination of the membrane (Yoshida et al., 2018); in the initial stage of CME (also defined as the 'growing phase'), the diameter and depth of the invagination increased as the signal intensity of clathrin increased (Fig. 2). Notably, both the clathrin signal and the pit diameter remained constant for a certain period (defined as the 'stable phase') after the initial growth (Fig. 2). These observations clearly fit the 'constant radius' model, rather than the 'constant area' model.

Furthermore, the use of HS-AFM has allowed us to identify and distinguish the different endocytic pathways, such as through clathrin, caveolae and CLICs. For instance, live-cell HS-AFM imaging of COS7 cells revealed a number of small invaginations or pits with an aperture varying from 80 nm to 400 nm and with varying persistence from a few seconds to minutes (Yoshida et al., 2018), which represent different endocytic structures or pathways. The correlative imaging (HS-AFM and CLSM) of COS7 cells simultaneously expressing clathrin and caveolin fused to fluorescent proteins successfully distinguished between these two different pathways, and revealed that CCPs had apertures ranging between 150 and 400 nm with an average duration of 81 s, whereas caveolae were smaller (between 80 and 120 nm in aperture) and longer lasting (more than 400 s) (Yoshida et al., 2018). By combining use of the technique with use of marker proteins for individual endocytic pathways, live-cell HS-AFM correlative imaging can specifically characterise the morphological changes in the plasma membrane for the pathway of interest.

Inhomogeneity of membrane morphologies at the closing step of CME

Recent applications of various fluorescence imaging techniques, including super-resolution microscopy (Arasada et al., 2018; Huang et al., 2008; Jones et al., 2011), as well as live-cell HS-AFM (Suzuki et al., 2013; Yoshida et al., 2015, 2018), have unveiled the molecular mechanisms of 'pit closing', which are different from what had been expected based on electron microscope images. The scission step proceeds with a deformation of the lipid bilayer at the neck of the pit, such that the two membranes are close to each other, followed by the fusion of the membranes (Higgins and McMahon, 2002). This complex process is thought to be mediated by dynamin, which binds to the neck of the pit and constricts the membrane until it fuses (Antonny et al., 2016; Kaksonen and Roux, 2018). However, knockout and knockdown experiments with dynamin 1 and -2 have demonstrated that they are not necessary for pit closing (Ferguson et al., 2009; Hinshaw, 2000; Park et al., 2013), suggesting an alternative mechanism for scission.

A study using ion conductance microscopy identified a unique membrane protrusion near the CCP that was present before the complete closing of the pit and that gradually covered the pit area
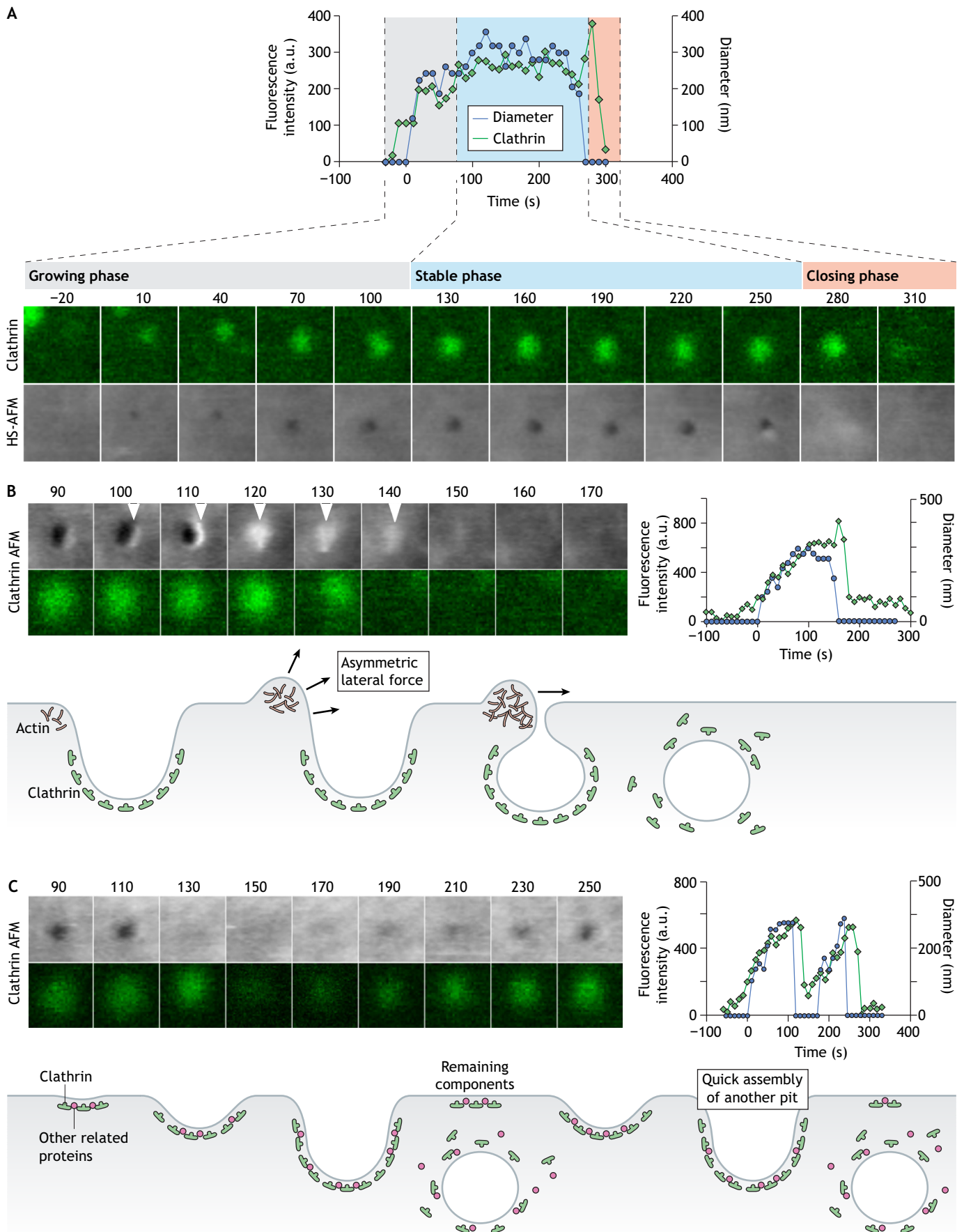
Fig. 2. See next page for legend.

Fig. 2. Correlative live-cell imaging of CME using HS-AFM and CLSM.
(A) Correlative imaging of CME with live-cell HS-AFM and CLSM. The fluorescence images (top) of EGFP–clathrin and AFM images (bottom) were obtained from a live COS7 cell every 10 s and shown here every 30 s, with 0 s representing the moment when the CCP could be clearly visualised by HS-AFM imaging. Image size: 1.2×1.2 µm^2. In the graph shown, the fluorescence intensity (green) and diameter of the membrane invagination in the AFM image (dotted black) are plotted against time. In the beginning, both the clathrin signal and the membrane invagination increased with time ('growing phase'). Eventually, both signals reached a plateau and remained constant for another period (10–120 s) ('stable phase'). Thereafter, the membrane invagination disappeared within 10 s, and the clathrin signal also vanished ('closing phase'). (B,C) Morphological variations of CME process observed by correlative HS-AFM. Correlative images obtained from CLSM and HS-AFM (top) and a schematic illustration (bottom) are shown. Fluorescence images of EGFP–clathrin and HS-AFM images were obtained from a live COS7 cell every 10 s. Image size: 1.2×1.2 µm^2. The graphs on the top right illustrate the change in fluorescence intensity (green) and diameter of the membrane invagination in the AFM image (dotted black) over time. (B) Time-lapse series illustrating actin-driven pit closing. Actin polymerises besides the pit and induces a local membrane protrusion, which drives an asymmetric closing motion of the pit. This is different from a previously accepted model of closing that involves a symmetric constriction of the membrane, mainly mediated by dynamin (Antonny et al., 2016; Kaksonen and Roux, 2018). Arrowheads in image highlight the position of membrane protrusion. (C) Time-lapse series supporting the 'hot-spot' model of CME. Two or more CCPs successively appear at the same position; after the first pit closed, a second pit appears at the same position within 10–70 s. The 'hot-spot' of CME could be observed in COS7 cells together with actin-driven pit closing but with lower frequency. A proportion of the clathrin and other related proteins, such as SNX9 (Nunez et al., 2011), remain on the plasma membrane after the scission of the CCP from the plasma membrane, which recruits clathrin and other proteins to the same location and gives rise to another CCP. Images and graphs shown are reproduced from Yoshida et al. (2018) where they were published under a CC-BY 4.0 license.

(Shevchuk et al., 2012). The generation of a membrane protrusion during the 'closing phase' of CME (defined by the gradual decrease of clathrin signal) was later confirmed by our correlative HS-AFM and CLSM approach (Fig. 2B) (Yoshida et al., 2018). Notably, this membrane protrusion occurred in more than 50% of the total CME events (Yoshida et al., 2018). These morphological observations suggest that this asymmetric membrane protrusion plays a dominant role in the closing process, which is distinct from the previously proposed symmetric 'constriction' mediated by dynamin (Antonny et al., 2016; Kaksonen and Roux, 2018). In addition, correlative imaging with GFP–Lifeact (fluorescently labelled actin), as well as inhibition of the Arp2/3 complex, which mediates branching of actin filaments, with CK666, demonstrated that the asymmetric membrane protrusion was induced by an accumulation of short branched actin filaments near the CCP (Yoshida et al., 2018). This observation is consistent with earlier EM images that found short and branched actin filaments next to CCPs (Collins et al., 2011). It can be speculated that an asymmetric closure might be more energetically favourable than symmetric constriction when the stiffness and tension of the plasma membrane are considered (Vasan et al., 2020). The involvement of actin in CME will be discussed below.

Another intriguing observation made by HS-AFM regarding CME is that two or more CCPs successively appear at the same position (observed in ~15% of total CCPs); after the first pit closes, a second pit appears at the same position within 10–70 s (Yoshida et al., 2018) (Fig. 2C). This might be due to either re-fusion of the released CCVs with the plasma membrane or the highly efficient assembly of another CME machinery at the same position. The latter is consistent with previously reported endocytic 'hot-spots', where multiple rounds of CME were found to occur in a limited area of the

membrane owing to the local enrichment of CME-related proteins (Nunez et al., 2011; Saffarian et al., 2009). Our correlative imaging with HS-AFM also supports the existence of such 'hot-spots', as the intensity of the clathrin signal is reduced after the pit closes and increases again when the pit reopens (Fig. 2C) (Yoshida et al., 2018); however, these results do not completely exclude the possibility of refusion of the released CCP and the plasma membrane. Further analysis using an imaging technique with higher z-resolution (e.g. super-resolution microscopy) may contribute to clarify the underlying mechanism behind the formation of 'hot-spots'.

Role of actin dynamics in CME

Several studies have demonstrated the involvement of actin in CME (Fujimoto et al., 2000; Grassart et al., 2014; Yarar et al., 2005). Indeed, the inhibition of actin dynamics with specific inhibitors (cytochalasin B, cytochalasin D, jasplakinolide and CK666) affected the progression of CME (Akamatsu et al., 2020; Fujimoto et al., 2000). As various membrane structures and cellular processes with membrane deformation, such as filopodia, lamellipodia and micropinocytosis, are mediated by actin-based structures, it is reasonable to assume that actin also regulates CME. However, the role of actin in the CME has remained controversial because the inhibition of actin dynamics by inhibitors cannot completely block endocytosis in animal cells (Fujimoto et al., 2000). Furthermore, the inhibition of actin dynamics in the cell cortex affects the tension of the plasma membrane and thus may indirectly alter the kinetics of membrane deformation (Diz-Muñoz et al., 2013). Here, we briefly summarise the role of actin in CME and the contribution of HS-AFM in addressing it.

Actin has been shown to participate in CME by bending the plasma membrane to promote the initiation of CCPs (Kukulski et al., 2012), by counteracting membrane tension to drive the invagination of the pit (Boulant et al., 2011) and by coordinating with other CCP-related proteins to assist the scission of the vesicle (Tsujita et al., 2006). Recent studies using super-resolution microscopy have revealed that actin nucleation at the CCP largely depends on a circular 'nano-template' formed by WASP proteins, which is necessary for highly efficient endocytosis (Mund et al., 2018). However, actin polymerisation from such a circular template is not sufficient to explain the actin-driven asymmetric membrane protrusions, implicating a more complex actin architecture in the area surrounding the CCP.

Moreover, cortical actin dynamics may play an important role in driving CCVs into the cytoplasm by either interacting with myosin, which is highly abundant in the cell cortex (Chandrasekar et al., 2014), or by accumulating between the plasma membrane and the vesicles to physically prevent the refusion of CCVs back to the membrane. Notably, our group revealed, by using live-cell HS-AFM, that actin polymerisation occurs mainly on the cytoplasmic surface of the plasma membrane, and the newly synthesised actin filaments descend into the interior of the cell, which generates an inward movement of the cortical filament network (Zhang et al., 2017). This mechanism may also contribute to the force driving CCPs into the cytoplasm.

Dynamics of the cortical actin network

Cortical actin filaments form a random skeletal network beneath the plasma membrane and play pivotal roles in various cellular events at the cell surface, including endocytosis, as well as in cell and tissue morphogenesis (Chalut and Paluch, 2016; Chikina et al., 2019; Chugh et al., 2017; Sekiya-Kawasaki et al., 2003). A number of
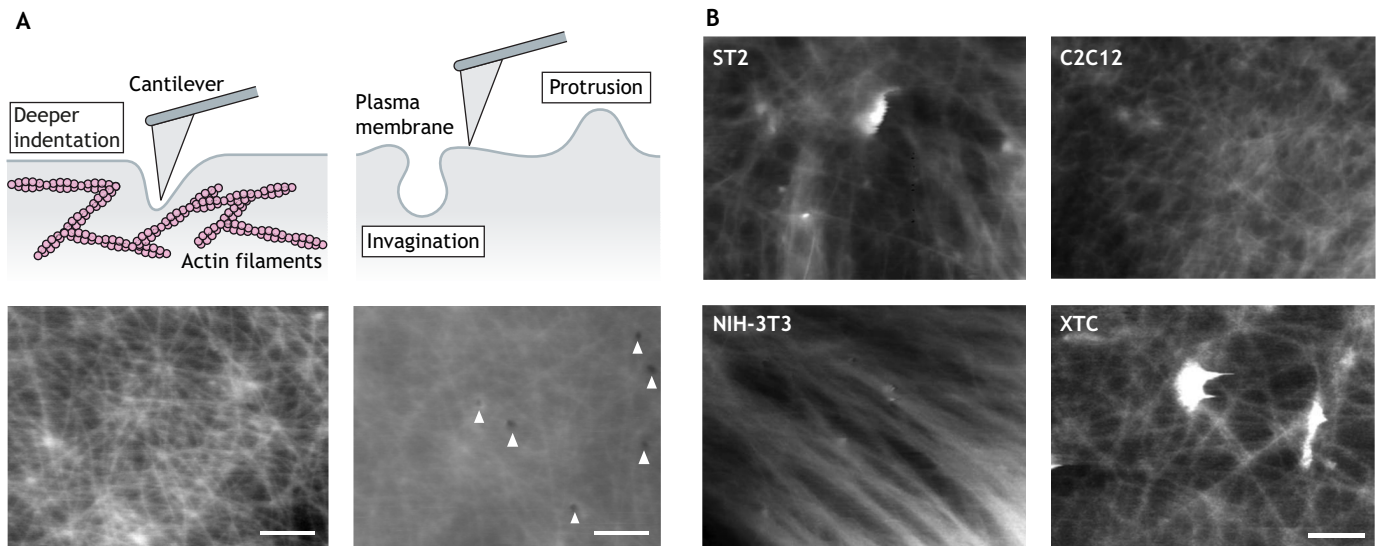
Fig. 3. Live-cell imaging of the plasma membrane and cortical actin using HS-AFM. (A) Schematic illustration of the experimental setup used to visualise either the plasma membrane (right) or cortical actin (left) using HS-AFM, with the relative position of the cantilever and plasma membrane. Representative HS-AFM images of COS7 cells are shown below. The positions of endocytosis events are indicated with arrowheads. Image size: 6.0×4.5 µm². Scale bars: 1 µm. (B) HS-AFM images of various cortical actin architectures in different cell lines. NIH-3T3 mouse embryonic fibroblast cells, C2C12 mouse myoblast cells, ST2 mouse bone marrow-derived stromal cells and XTC frog fibroblast cells are shown. Clear differences can be observed in the density, orientation, length, and polymerization rate of the filaments. See Zhang et al. (2017) for a detailed analysis of the respective structures. Image size: 6.0×4.5 µm². Scale bar: 1 µm. Images reproduced from Zhang et al. (2017) by permission of Oxford University Press and The Japanese Society of Microscopy.

previous studies using various fluorescence imaging techniques have revealed the dynamics of actin in lamellipodia, filopodia and stress fibres (Aroush et al., 2017; Medalia et al., 2007; Peterson et al., 2004). However, in contrast to stress fibers and filopodia, both of which are composed of a thick bundle of actin filaments, the morphological observation of individual filaments of cortical actin in a living cell has been a difficult task because of the dense and random arrangement of actin filaments, and rapid polymerization/depolymerization dynamics (Aroush et al., 2017; Svitkina, 2020; Tobacman and Korn, 1983). Although tapping mode AFM has been applied to quantify the density of cortical actin (Eghiaian et al., 2015; Kronlage et al., 2015), imaging of individual actin filaments in the living cell cortex by conventional AFM has not been successful because of its slow scanning rate and the large force that generated by a large cantilever probe.

We successfully observed individual actin filaments in the cell cortex by live-cell HS-AFM by indenting the cantilever probe slightly deeper into the cell than during the imaging of the plasma membrane (Fig. 3A), which allowed the visualisation of actin filaments, which are stiffer than the lipid bilayer, with high contrast (Zhang et al., 2017). The process of 'filament elongation' (190 nm/s) was successfully captured, supporting the fact that the filament observed here is indeed a single actin filament (Zhang et al., 2017), although the apparent width of the filament was wider than that of a single actin filament (∼7 nm) owing to it being observed through the lipid bilayer. Treatment with cytochalasin B, which binds to the barbed end of F-actin and blocks actin polymerisation (Theodoropoulos et al., 1994), markedly decreased the polymerisation rate and the density of the filaments (Zhang et al., 2017). In contrast, jasplakinolide can be used to inhibit actin depolymerisation and stabilise F-actin (Bubb et al., 2000). HS-AFM imaging revealed that treatment with jasplakinolide decreased the actin polymerisation rate without affecting the density of the meshwork (Zhang et al., 2017).

Based on the observed polymerisation rate and the previously reported rate constant ($\sim$110 s^{-1}) (Pollard, 1986), the concentration of free G-actin in the cell cortex has been estimated to be ∼7 µM (Zhang et al., 2017), which is lower than the previous estimates obtained through biochemical approaches (∼30 µM) (Goode and Eck, 2007). These results point to several intriguing aspects of the intracellular actin pool. First, the free G-actin pool may be different in different parts of the cell. It can be speculated that the cell cortex, where actin polymerisation actively occurs and is mediated by actin-regulatory proteins (Bovellan et al., 2014), contains a relatively small amount of free G-actin, whereas there are larger amounts of G-actin in the cytoplasm. Alternatively, a large amount of G-actin may be sequestered by thymosin β4 and not be actively involved in turnover (Xue et al., 2014). The observation that overexpression of thymosin β4 did not affect the turnover of cortical actin (Zhang et al., 2017) might support this notion. Taken together, the insights into actin dynamics in a living cell obtained from HS-AFM, together with information from other single-molecule studies *in vitro* and biochemical approaches, clearly contribute to our understanding of the molecular dynamics and kinetics of actin turnover in the intracellular milieu.

Spatiotemporal regulation of various actin-based architectures

One of the most intriguing aspects of intracellular actin-based structures is how such a variety of architectures is spatiotemporally regulated by a variety of regulatory proteins (Blanchoin et al., 2014; Bovellan et al., 2014; Roffers-Agarwal et al., 2005). The polymerisation and depolymerisation of actin are regulated by a large number of proteins that modulate nucleation, elongation and severing (Pollard, 2016). In addition, the higher-order architectures of actin filaments are also regulated by various crosslinkers and bundlers (Tilney et al., 1998). Furthermore, the activities of these regulatory proteins are controlled by complex signalling pathways,

including kinases and small GTPases, such as RhoA, Rac1 and Cdc42 (Lee and Dominguez, 2010; Moujaber and Stochaj, 2020). For example, actin dynamics in lamellipodia, which are directly coupled to cell motility and are regulated by actin nucleators and small GTPases, can be visualised by various single-molecule observation techniques, as well as HS-AFM (Higashida et al., 2013; Ponti et al., 2004). Integrating information from fluorescence-based techniques, EM and HS-AFM together with other molecular and cellular biological techniques will contribute to the understanding of such regulation.

A variety of cortical actin networks and their dynamics in different cell lines can be visualised by using HS-AFM (Fig. 3B) (Zhang et al., 2017). A clearly visible actin mesh was observed in mouse bone-marrow-derived stromal cells (ST2), mouse myoblasts (C2C12) cells and frog fibroblast (XTC) cells, whereas large actin bundles along the long axis of the cell are found in mouse embryonic fibroblast (NIH3T3) cells (Zhang et al., 2017). A comparison of microscopic images obtained by EM and live-cell HS-AFM implies that cortical actin structures are different in different parts of the cell (Svitkina, 2020). For example, the actin network at the basal surface of a cultured cell as determined by EM (Morone et al., 2006; Svitkina, 2020) contains denser actin filaments than at the apical surface as observed by AFM (Eghiaian et al., 2015; Kronlage et al., 2015). This might be because the basal surface contains a number of actin-based structures, such as focal adhesions and stress fibres, in order to adhere to the substrate (Burridge and Guilluy, 2016). Lamellipodia also contain a denser actin network than the apical surface (Aroush et al., 2017; Svitkina, 2018). Combination of microscopic imaging with biochemical approaches will be required to elucidate how these actin-based structures are constructed and regulated by various actin-regulatory proteins in different parts of the cell.

A dynamic view of the cortical actin network is highly justified, yet difficult to investigate owing to the lack of imaging techniques with adequate spatiotemporal resolutions. In this context, live-cell HS-AFM is clearly able to visualise the dynamics of a single actin filament and describe the role of actin-related proteins in mediating the morphological features of the actin cortex. We believe that this approach will provide a valuable platform for resolving the physical structure as well as the biological significance of cortical actin.

Conclusions and perspectives

The application of HS-AFM in live-cell imaging provides us with the possibility of directly visualising nanoscale structures and events on and beneath the plasma membrane. Here, we have summarised the brief history of HS-AFM and its application in live mammalian cells, with special emphasis on the morphological changes in the plasma membrane during CME and the dynamics of cortical actin. In particular, live-cell correlative imaging with CLSM is one of the most powerful applications of HS-AFM, which compensates for the disadvantages of both microscopies and produces morphological information as well as determining protein localisation in a living cell. The spatiotemporal resolution of HS-AFM continues to improve, and various applications are also under development as outlined below.

One of the possible applications of correlative HS-AFM imaging is the visualisation of viral infection and budding. The plasma membrane is the place where viruses make the first contact with a host cell and, in some enveloped viruses, viral proteins and genomes are assembled and packaged into a virion using the plasma membrane as a coating. It is well known that interactions between

the cell cortex (plasma membrane, membrane proteins and cortical cytoskeleton) and viral proteins have crucial roles in viral infection and budding processes (Barman and Nayak, 2007; Gladnikoff et al., 2009; Harmon et al., 2010; Iliopoulou et al., 2018). Therefore, HS-AFM together with fluorescence microscopy could be a feasible technique to visualise the dynamic behaviour of viruses at the cell surface and help to reveal the molecular mechanism of viral infection and budding.

Although live-cell HS-AFM has provided new information regarding membrane-related structures and cellular events, the temporal resolution of the current HS-AFM system still limits its broader application, such as in fast or ultrafast endocytic processes that have a total lifetime of within a few seconds and function more efficiently than CME in the internalisation of cargo molecules (Watanabe and Boucrot, 2017). For this purpose, further improvement in the temporal resolution without reducing the scanning area is necessary. To improve the spatial resolution of correlative imaging, HS-AFM can be combined with super-resolution microscopy. Current super-resolution techniques can provide spatial resolutions of up to ∼10 nm in the lateral dimension and 50 nm in the vertical dimension, which is comparable to that of HS-AFM (∼5 nm in the lateral dimension and <1 nm in the vertical dimension). It is anticipated that the combination of these two techniques will allow us to reconstruct the three-dimensional structures of small membrane protrusions and invaginations, such as caveolae or synaptic vesicles, as well as follow the assembly of associated proteins at the corresponding location with high precision. In that respect, combining correlative imaging with HS-AFM, and perhaps other imaging techniques in the future has the potential to elucidate molecular mechanisms in a way that is not currently not attainable by other approaches.

References
Akamatsu, M., Vasan, R., Serwas, D., Ferrin, M. A., Rangamani, P. and Drubin, D. G. (2020). Principles of self-organization and load adaptation by the actin cytoskeleton during clathrin-mediated endocytosis. *eLife* **9**, e49840. doi:10.7554/eLife.49840

Akita, S., Nishijima, H., Nakayama, Y., Tokumasu, F. and Takeyasu, K. (1999). Carbon nanotube tips for a scanning probe microscope: their fabrication and properties. *J. Phys. D* **32**, 1044. doi:10.1088/0022-3727/32/9/316

Ando, T. (2018). High-speed atomic force microscopy and its future prospects. *Biophys. Rev.* **10**, 285-292. doi:10.1007/s12551-017-0356-5

Ando, T., Kodera, N., Takai, E., Maruyama, D., Saito, K. and Toda, A. (2001). A high-speed atomic force microscope for studying biological macromolecules. *Proc. Natl. Acad. Sci. USA* **98**, 12468-12472. doi:10.1073/pnas.211400898

Ando, T., Uchihashi, T. and Fukuma, T. (2008). High-speed atomic force microscopy for nano-visualization of dynamic biomolecular processes. *Prog. Surf. Sci.* **83**, 337-437. doi:10.1016/j.progsurf.2008.09.001

Antonny, B., Burd, C., De Camilli, P., Chen, E., Daumke, O., Faelber, K., Ford, M., Frolov, V. A., Frost, A., Hinshaw, J. E. et al. (2016). Membrane fission by dynamin: what we know and what we need to know. *EMBO J.* **35**, 2270-2284. doi:10.15252/embj.201694613

Arasada, R., Sayyad, W. A., Berro, J. and Pollard, T. D. (2018). High-speed superresolution imaging of the proteins in fission yeast clathrin-mediated endocytic actin patches. *Mol. Biol. Cell* **29**, 295-303. doi:10.1091/mbc.E17-06-0415

Aroush, D. R.-B., Ofer, N., Abu-Shah, E., Allard, J., Krichevsky, O., Mogilner, A. and Keren, K. (2017). Actin turnover in lamellipodial fragments. *Curr. Biol.* **27**, 2963-2973.e14. doi:10.1016/j.cub.2017.08.066

Barman, S. and Nayak, D. P. (2007). Lipid raft disruption by cholesterol depletion enhances influenza A virus budding from MDCK cells. *J. Virol.* **81**, 12169-12178. doi:10.1128/JVI.00835-07

Binnig, G., Quate, C. F. and Gerber, C. (1986). Atomic force microscope. *Phys. Rev. Lett.* **56**, 930. doi:10.1103/PhysRevLett.56.930

Blanchoin, L., Boujemaa-Paterski, R., Sykes, C. and Plastino, J. (2014). Actin dynamics, architecture, and mechanics in cell motility. *Physiol. Rev.* **94**, 235-263. doi:10.1152/physrev.00018.2013

Boulant, S., Kural, C., Zeeh, J.-C., Ubelmann, F. and Kirchhausen, T. (2011). Actin dynamics counteract membrane tension during clathrin-mediated endocytosis. *Nat. Cell Biol.* **13**, 1124-1131. doi:10.1038/ncb2307

Bovellan, M., Romeo, Y., Biro, M., Boden, A., Chugh, P., Yonis, A., Vaghela, M., Fritzsche, M., Moulding, D., Thorogate, R. et al. (2014). Cellular control of cortical actin nucleation. *Curr. Biol.* **24**, 1628-1635. doi:10.1016/j.cub.2014.05.069

Bubb, M. R., Spector, I., Beyer, B. B. and Fosen, K. M. (2000). Effects of jasplakinolide on the kinetics of actin polymerization: an explanation for certain in vivo observations. *J. Biol. Chem.* **275**, 5163-5170. doi:10.1074/jbc.275.7.5163

Burridge, K. and Guilluy, C. (2016). Focal adhesions, stress fibers and mechanical tension. *Exp. Cell Res.* **343**, 14-20. doi:10.1016/j.yexcr.2015.10.029

Casuso, I., Khao, J., Chami, M., Paul-Gilloteaux, P., Husain, M., Duneau, J.-P., Stahlberg, H., Sturgis, J. N. and Scheuring, S. (2012). Characterization of the motion of membrane proteins using high-speed atomic force microscopy. *Nat. Nanotechnol.* **7**, 525-529. doi:10.1038/nnano.2012.109

Chalut, K. J. and Paluch, E. K. (2016). The actin cortex: a bridge between cell shape and function. *Dev. Cell* **38**, 571-573. doi:10.1016/j.devcel.2016.09.011

Chandrasekar, I., Goeckeler, Z. M., Turney, S. G., Wang, P., Wysolmerski, R. B., Adelstein, R. S. and Bridgman, P. C. (2014). Nonmuscle Myosin II Is a critical regulator of clathrin-mediated endocytosis. *Traffic* **15**, 418-432. doi:10.1111/tra.12152

Chen, H., Fre, S., Slepnev, V. I., Capua, M. R., Takei, K., Butler, M. H., Di Fiore, P. P. and De Camilli, P. (1998). Epsin is an EH-domain-binding protein implicated in clathrin-mediated endocytosis. *Nature* **394**, 793-797. doi:10.1038/29555

Chikina, A. S., Svitkina, T. M. and Alexandrova, A. Y. (2019). Time-resolved ultrastructure of the cortical actin cytoskeleton in dynamic membrane blebs. *J. Cell Biol.* **218**, 445-454. doi:10.1083/jcb.201806075

Chugh, P., Clark, A. G., Smith, M. B., Cassani, D. A. D., Dierkes, K., Ragab, A., Roux, P. P., Charras, G., Salbreux, G. and Paluch, E. K. (2017). Actin cortex architecture regulates cell surface tension. *Nat. Cell Biol.* **19**, 689-697. doi:10.1038/ncb3525

Collins, A., Warrington, A., Taylor, K. A. and Svitkina, T. (2011). Structural organization of the actin cytoskeleton at sites of clathrin-mediated endocytosis. *Curr. Biol.* **21**, 1167-1175. doi:10.1016/j.cub.2011.05.048

Diz-Muñoz, A., Fletcher, D. A. and Weiner, O. D. (2013). Use the force: membrane tension as an organizer of cell shape and motility. *Trends Cell Biol.* **23**, 47-53. doi:10.1016/j.tcb.2012.09.006

Edstrom, R. D., Meinke, M. H., Yang, X., Yang, R., Elings, V. and Evans, D. F. (1990). Direct visualization of phosphorylase-phosphorylase kinase complexes by scanning tunneling and atomic force microscopy. *Biophys. J.* **58**, 1437-1448. doi:10.1016/S0006-3495(90)82489-9

Eghiaian, F., Rigato, A. and Scheuring, S. (2015). Structural, mechanical, and dynamical variability of the actin cortex in living cells. *Biophys. J.* **108**, 1330-1340. doi:10.1016/j.bpj.2015.01.016

Endo, M., Yang, Y., Suzuki, Y., Hidaka, K. and Sugiyama, H. (2012). Single-molecule visualization of the hybridization and dissociation of photoresponsive oligonucleotides and their reversible switching behavior in a DNA nanostructure. *Angew. Chem. Int. Ed.* **51**, 10518-10522. doi:10.1002/anie.201205247

Ferguson, S., Raimondi, A., Paradise, S., Shen, H., Mesaki, K., Ferguson, A., Destaing, O., Ko, G., Takasaki, J., Cremona, O. et al. (2009). Coordinated actions of actin and BAR proteins upstream of dynamin at endocytic clathrin-coated pits. *Dev. Cell* **17**, 811-822. doi:10.1016/j.devcel.2009.11.005

Flannagan, R. S., Jaumouillé, V. and Grinstein, S. (2012). The cell biology of phagocytosis. *Annu. Rev. Pathol.* **7**, 61-98. doi:10.1146/annurev-pathol-011811-132445

Fujimoto, L. M., Roth, R., Heuser, J. E. and Schmid, S. L. (2000). Actin assembly plays a variable, but not obligatory role in receptor-mediated endocytosis. *Traffic* **1**, 161-171. doi:10.1034/j.1600-0854.2000.010208.x

Giessibl, F. J. (2003). Advances in atomic force microscopy. *Rev. Mod. Phys.* **75**, 949. doi:10.1103/RevModPhys.75.949

Gilmore, J. L., Suzuki, Y., Tamulaitis, G., Siksnys, V., Takeyasu, K. and Lyubchenko, Y. L. (2009). Single-molecule dynamics of the DNA– Eco RII protein complexes revealed with high-speed atomic force microscopy. *Biochemistry* **48**, 10492-10498. doi:10.1021/bi9010368

Gladnikoff, M., Shimoni, E., Gov, N. S. and Rousso, I. (2009). Retroviral assembly and budding occur through an actin-driven mechanism. *Biophys. J.* **97**, 2419-2428. doi:10.1016/j.bpj.2009.08.016

Goode, B. L. and Eck, M. J. (2007). Mechanism and function of formins in the control of actin assembly. *Annu. Rev. Biochem.* **76**, 593-627. doi:10.1146/annurev.biochem.75.103004.142647

Grassart, A., Cheng, A. T., Hong, S. H., Zhang, F., Zenzer, N., Feng, Y., Briner, D. M., Davis, G. D., Malkov, D. and Drubin, D. G. (2014). Actin and dynamin2 dynamics and interplay during clathrin-mediated endocytosis. *J. Cell Biol.* **205**, 721-735. doi:10.1083/jcb.201403041

Guthold, M., Falvo, M., Matthews, W. G., Paulson, S., Mullin, J., Lord, S., Erie, D., Washburn, S., Superfine, R., Brooks, F. P.Jr. et al. (1999). Investigation and modification of molecular structures with the nanoManipulator. *J. Mol. Graph. Model.* **17**, 187-197. doi:10.1016/S1093-3263(99)00030-3

Hansma, P., Elings, V., Marti, O. and Bracker, C. (1988). Scanning tunneling microscopy and atomic force microscopy: application to biology and technology. *Science* **242**, 209-216. doi:10.1126/science.3051380

Harmon, B., Campbell, N. and Ratner, L. (2010). Role of Abl kinase and the Wave2 signaling complex in HIV-1 entry at a post-hemifusion step. *PLoS Pathog.* **6**, e1000956. doi:10.1371/journal.ppat.1000956

Higashida, C., Kiuchi, T., Akiba, Y., Mizuno, H., Maruoka, M., Narumiya, S., Mizuno, K. and Watanabe, N. (2013). F-and G-actin homeostasis regulates mechanosensitive actin nucleation by formins. *Nat. Cell Biol.* **15**, 395-405. doi:10.1038/ncb2693

Higgins, M. K. and McMahon, H. T. (2002). Snap-shots of clathrin-mediated endocytosis. *Trends Biochem. Sci.* **27**, 257-263. doi:10.1016/S0968-0004(02)02089-3

Hinshaw, J. E. (2000). Dynamin and its role in membrane fission. *Annu. Rev. Cell Dev. Biol.* **16**, 483-519. doi:10.1146/annurev.cellbio.16.1.483

Howes, M. T., Mayor, S. and Parton, R. G. (2010). Molecules, mechanisms, and cellular roles of clathrin-independent endocytosis. *Curr. Opin. Cell Biol.* **22**, 519-527. doi:10.1016/j.ceb.2010.04.001

Huang, B., Wang, W., Bates, M. and Zhuang, X. (2008). Three-dimensional super-resolution imaging by stochastic optical reconstruction microscopy. *Science* **319**, 810-813. doi:10.1126/science.1153529

Igarashi, K., Uchihashi, T., Koivula, A., Wada, M., Kimura, S., Okamoto, T., Penttilä, M., Ando, T. and Samejima, M. (2011). Traffic jams reduce hydrolytic efficiency of cellulase on cellulose surface. *Science* **333**, 1279-1282. doi:10.1126/science.1208386

Iliopoulou, M., Nolan, R., Alvarez, L., Watanabe, Y., Coomer, C. A., Jakobsdottir, G. M., Bowden, T. A. and Padilla-Parra, S. (2018). A dynamic three-step mechanism drives the HIV-1 pre-fusion reaction. *Nat. Struct. Mol. Biol.* **25**, 814-822. doi:10.1038/s41594-018-0113-x

Jones, S. A., Shim, S.-H., He, J. and Zhuang, X. (2011). Fast, three-dimensional super-resolution imaging of live cells. *Nat. Methods* **8**, 499. doi:10.1038/nmeth.1605

Kaksonen, M. and Roux, A. (2018). Mechanisms of clathrin-mediated endocytosis. *Nat. Rev. Mol. Cell Biol.* **19**, 313. doi:10.1038/nrm.2017.132

Kasas, S., Thomson, N. H., Smith, B. L., Hansma, P. K., Miklossy, J. and Hansma, H. G. (1997). Biological applications of the AFM: from single molecules to organs. *Int. J. Imaging Syst. Technol.* **8**, 151-161. doi:10.1002/(SICI)1098-1098(1997)8:2<151::AID-IMA2>3.0.CO;2-9

Kobayashi, K., Kodera, N., Kasai, T., Tahara, Y. O., Toyonaga, T., Mizutani, M., Fujiwara, I., Ando, T. and Miyata, M. (2021). Movements of Mycoplasma mobile gliding machinery detected by high-speed atomic force microscopy. *Mbio* **12**, e0004021. doi:10.1128/mBio.00040-21

Kodera, N., Yamamoto, D., Ishikawa, R. and Ando, T. (2010). Video imaging of walking myosin V by high-speed atomic force microscopy. *Nature* **468**, 72-76. doi:10.1038/nature09450

Kronlage, C., Schäfer-Herte, M., Böning, D., Oberleithner, H. and Fels, J. (2015). Feeling for filaments: quantification of the cortical actin web in live vascular endothelium. *Biophys. J.* **109**, 687-698. doi:10.1016/j.bpj.2015.06.066

Kukulski, W., Schorb, M., Kaksonen, M. and Briggs, J. A. G. (2012). Plasma membrane reshaping during endocytosis is revealed by time-resolved electron tomography. *Cell* **150**, 508-520. doi:10.1016/j.cell.2012.05.046

Lee, S. H. and Dominguez, R. (2010). Regulation of actin cytoskeleton dynamics in cells. *Mol. Cells* **29**, 311-325. doi:10.1007/s10059-010-0053-8

Leuba, S. H., Yang, G., Robert, C., Samori, B., van Holde, K., Zlatanova, J. and Bustamante, C. (1994). Three-dimensional structure of extended chromatin fibers as revealed by tapping-mode scanning force microscopy. *Proc. Natl. Acad. Sci. USA* **91**, 11621-11625. doi:10.1073/pnas.91.24.11621

Martin, Y., Williams, C. C. and Wickramasinghe, H. K. (1987). Atomic force microscope–force mapping and profiling on a sub 100-Å scale. *J. Appl. Phys.* **61**, 4723-4729. doi:10.1063/1.338807

McMahon, H. T. and Boucrot, E. (2011). Molecular mechanism and physiological functions of clathrin-mediated endocytosis. *Nat. Rev. Mol. Cell Biol.* **12**, 517-533. doi:10.1038/nrm3151

Medalia, O., Beck, M., Ecke, M., Weber, I., Neujahr, R., Baumeister, W. and Gerisch, G. (2007). Organization of actin networks in intact filopodia. *Curr. Biol.* **17**, 79-84. doi:10.1016/j.cub.2006.11.022

Merrifield, C. J., Perrais, D. and Zenisek, D. (2005). Coupling between clathrin-coated-pit invagination, cortactin recruitment, and membrane scission observed in live cells. *Cell* **121**, 593-606. doi:10.1016/j.cell.2005.03.015

Minne, S. C., Yaralioglu, G., Manalis, S. R., Adams, J. D., Zesch, J., Atalar, A. and Quate, C. F. (1998). Automated parallel high-speed atomic force microscopy. *Appl. Phys. Lett.* **72**, 2340-2342. doi:10.1063/1.121353

Morone, N., Fujiwara, T., Murase, K., Kasai, R. S., Ike, H., Yuasa, S., Usukura, J. and Kusumi, A. (2006). Three-dimensional reconstruction of the membrane skeleton at the plasma membrane interface by electron tomography. *J. Cell Biol.* **174**, 851-862. doi:10.1083/jcb.200606007

Moujaber, O. and Stochaj, U. (2020). The cytoskeleton as regulator of cell signaling pathways. *Trends Biochem. Sci.* **45**, 96-107. doi:10.1016/j.tibs.2019.11.003

Mund, M., van der Beek, J. A., Deschamps, J., Dmitrieff, S., Hoess, P., Monster, J. L., Picco, A., Nédélec, F., Kaksonen, M. and Ries, J. (2018). Systematic nanoscale analysis of endocytosis links efficient vesicle formation to patterned actin nucleation. *Cell* **174**, 884-896.e17. doi:10.1016/j.cell.2018.06.032

Nunez, D., Antonescu, C., Mettlen, M., Liu, A., Schmid, S. L., Loerke, D. and Danuser, G. (2011). Hotspots organize clathrin-mediated endocytosis by efficient recruitment and retention of nucleating resources. *Traffic* **12**, 1868-1878. doi:10.1111/j.1600-0854.2011.01273.x

Oberleithner, H., Brinckmann, E., Giebisch, G. and Geibel, J. (1995). Visualizing life on biomembranes by atomic force microscopy. *Kidney Int.* **48**, 923-929. doi:10.1038/ki.1995.373

Park, R. J., Shen, H., Liu, L., Liu, X., Ferguson, S. M. and De Camilli, P. (2013). Dynamin triple knockout cells reveal off target effects of commonly used dynamin inhibitors. *J. Cell Sci.* **126**, 5305-5312. doi:10.1242/jcs.138578

Peterson, L. J., Rajfur, Z., Maddox, A. S., Freel, C. D., Chen, Y., Edlund, M., Otey, C. and Burridge, K. (2004). Simultaneous stretching and contraction of stress fibers in vivo. *Mol. Biol. Cell* **15**, 3497-3508. doi:10.1091/mbc.e03-09-0696

Pollard, T. D. (1986). Rate constants for the reactions of ATP-and ADP-actin with the ends of actin filaments. *J. Cell Biol.* **103**, 2747-2754. doi:10.1083/jcb.103.6.2747

Pollard, T. D. (2016). Actin and actin-binding proteins. *Cold Spring Harb. Perspect. Biol.* **8**, a018226. doi:10.1101/cshperspect.a018226

Ponti, A., Machacek, M., Gupton, S. L., Waterman-Storer, C. M. and Danuser, G. (2004). Two distinct actin networks drive the protrusion of migrating cells. *Science* **305**, 1782-1786. doi:10.1126/science.1100533

Putman, C. A. J., Van der Werf, K. O., De Grooth, B. G., Van Hulst, N. F. and Greve, J. (1994). Tapping mode atomic force microscopy in liquid. *Appl. Phys. Lett.* **64**, 2454-2456. doi:10.1063/1.111597

Roffers-Agarwal, J., Xanthos, J. B. and Miller, J. R. (2005). Regulation of actin cytoskeleton architecture by Eps8 and Abi1. *BMC Cell Biol.* **6**, 36. doi:10.1186/1471-2121-6-36

Royle, S. J. and Lagnado, L. (2003). Endocytosis at the synaptic terminal. *J. Physiol.* **553**, 345-355. doi:10.1113/jphysiol.2003.049221

Sabharanjak, S., Sharma, P., Parton, R. G. and Mayor, S. (2002). GPI-anchored proteins are delivered to recycling endosomes via a distinct cdc42-regulated, clathrin-independent pinocytic pathway. *Dev. Cell* **2**, 411-423. doi:10.1016/S1534-5807(02)00145-4

Saffarian, S., Cocucci, E. and Kirchhausen, T. (2009). Distinct dynamics of endocytic clathrin-coated pits and coated plaques. *PLoS Biol.* **7**, e1000191. doi:10.1371/journal.pbio.1000191

Sanchez, H., Suzuki, Y., Yokokawa, M., Takeyasu, K. and Wyman, C. (2011). Protein–DNA interactions in high speed AFM: single molecule diffusion analysis of human RAD54. *Integr. Biol.* **3**, 1127-1134. doi:10.1039/c1ib00039j

Sannohe, Y., Endo, M., Katsuda, Y., Hidaka, K. and Sugiyama, H. (2010). Visualization of dynamic conformational switching of the G-quadruplex in a DNA nanostructure. *J. Am. Chem. Soc.* **132**, 16311-16313. doi:10.1021/ja1058907

Sekiya-Kawasaki, M., Groen, A. C., Cope, M. J. T. V., Kaksonen, M., Watson, H. A., Zhang, C., Shokat, K. M., Wendland, B., McDonald, K. L., McCaffery, J. M. et al. (2003). Dynamic phosphoregulation of the cortical actin cytoskeleton and endocytic machinery revealed by real-time chemical genetic analysis. *J. Cell Biol.* **162**, 765-772. doi:10.1083/jcb.200305077

Shevchuk, A. I., Novak, P., Taylor, M., Diakonov, I. A., Ziyadeh-Isleem, A., Bitoun, M., Guicheney, P., Lab, M. J., Gorelik, J., Merrifield, C. J. et al. (2012). An alternative mechanism of clathrin-coated pit closure revealed by ion conductance microscopy. *J. Cell Biol.* **197**, 499-508. doi:10.1083/jcb.201109130

Shimada, A., Niwa, H., Tsujita, K., Suetsugu, S., Nitta, K., Hanawa-Suetsugu, K., Akasaka, R., Nishino, Y., Toyama, M., Chen, L. et al. (2007). Curved EFC/F-BAR-domain dimers are joined end to end into a filament for membrane invagination in endocytosis. *Cell* **129**, 761-772. doi:10.1016/j.cell.2007.03.040

Sulchek, T., Minne, S. C., Adams, J. D., Fletcher, D. A., Atalar, A., Quate, C. F. and Adderton, D. M. (1999). Dual integrated actuators for extended range high speed atomic force microscopy. *Appl. Phys. Lett.* **75**, 1637-1639. doi:10.1063/1.124779

Suzuki, Y., Gilmore, J. L., Yoshimura, S. H., Henderson, R. M., Lyubchenko, Y. L. and Takeyasu, K. (2011). Visual analysis of concerted cleavage by type IIF restriction enzyme SfiI in subsecond time region. *Biophys. J.* **101**, 2992-2998. doi:10.1016/j.bpj.2011.09.064

Suzuki, Y., Sakai, N., Yoshida, A., Uekusa, Y., Yagi, A., Imaoka, Y., Ito, S., Karaki, K. and Takeyasu, K. (2013). High-speed atomic force microscopy combined with inverted optical microscopy for studying cellular events. *Sci. Rep.* **3**, 2131. doi:10.1038/srep02131

Svitkina, T. (2018). The actin cytoskeleton and actin-based motility. *Cold Spring Harb. Perspect. Biol.* **10**, a018267. doi:10.1101/cshperspect.a018267

Svitkina, T. M. (2020). Actin cell cortex: structure and molecular organization. *Trends Cell Biol.* **30**, 556-565. doi:10.1016/j.tcb.2020.03.005

Swanson, J. A. and Watts, C. (1995). Macropinocytosis. *Trends Cell Biol.* **5**, 424-428. doi:10.1016/S0962-8924(00)89101-1

Taylor, M. J., Perrais, D. and Merrifield, C. J. (2011). A high precision survey of the molecular dynamics of mammalian clathrin-mediated endocytosis. *PLoS Biol.* **9**, e1000604. doi:10.1371/journal.pbio.1000604

Theodoropoulos, P. A., Gravanis, A., Tsapara, A., Margioris, A. N., Papadogiorgaki, E., Galanopoulos, V. and Stournaras, C. (1994). Cytochalasin B may shorten actin filaments by a mechanism independent of barbed end capping. *Biochem. Pharmacol.* **47**, 1875-1881. doi:10.1016/0006-2952(94)90318-2

Tilney, L. G., Connelly, P. S., Vranich, K. A., Shaw, M. K. and Guild, G. M. (1998). Why are two different cross-linkers necessary for actin bundle formation in vivo and what does each cross-link contribute? *J. Cell Biol.* **143**, 121-133. doi:10.1083/jcb.143.1.121

Tobacman, L. S. and Korn, E. D. (1983). The kinetics of actin nucleation and polymerization. *J. Biol. Chem.* **258**, 3207-3214. doi:10.1016/S0021-9258(18)32850-3

Tsujita, K., Suetsugu, S., Sasaki, N., Furutani, M., Oikawa, T. and Takenawa, T. (2006). Coordination between the actin cytoskeleton and membrane deformation by a novel membrane tubulation domain of PCH proteins is involved in endocytosis. *J. Cell Biol.* **172**, 269-279. doi:10.1083/jcb.200508091

Uchihashi, T., Iino, R., Ando, T. and Noji, H. (2011). High-speed atomic force microscopy reveals rotary catalysis of rotorless F1-ATPase. *Science* **333**, 755-758. doi:10.1126/science.1205510

Uchihashi, T., Watanabe, H., Fukuda, S., Shibata, M. and Ando, T. (2016). Functional extension of high-speed AFM for wider biological applications. *Ultramicroscopy* **160**, 182-196. doi:10.1016/j.ultramic.2015.10.017

Vasan, R., Rudraraju, S., Akamatsu, M., Garikipati, K. and Rangamani, P. (2020). A mechanical model reveals that non-axisymmetric buckling lowers the energy barrier associated with membrane neck constriction. *Soft Mat.* **16**, 784-797. doi:10.1039/C9SM01494B

Viani, M. B., Schäffer, T. E., Chand, A., Rief, M., Gaub, H. E. and Hansma, P. K. (1999). Small cantilevers for force spectroscopy of single molecules. *J. Appl. Phys.* **86**, 2258-2262. doi:10.1063/1.371039

Walters, D. A., Cleveland, J. P., Thomson, N. H., Hansma, P. K., Wendman, M. A., Gurley, G. and Elings, V. (1996). Short cantilevers for atomic force microscopy. *Rev. Sci. Instrum.* **67**, 3583-3590. doi:10.1063/1.1147177

Wang, H. and Clapham, D. E. (1999). Conformational changes of the in situ nuclear pore complex. *Biophys. J.* **77**, 241-247. doi:10.1016/S0006-3495(99)76885-2

Watanabe, S. and Boucrot, E. (2017). Fast and ultrafast endocytosis. *Curr. Opin. Cell Biol.* **47**, 64–71. doi:10.1016/j.ceb.2017.02.013

Watanabe, H., Uchihashi, T., Kobashi, T., Shibata, M., Nishiyama, J., Yasuda, R. and Ando, T. (2013). Wide-area scanner for high-speed atomic force microscopy. *Rev. Sci. Instrum.* **84**, 053702. doi:10.1063/1.4803449

Weinberg, J. and Drubin, D. G. (2012). Clathrin-mediated endocytosis in budding yeast. *Trends Cell Biol.* **22**, 1-13. doi:10.1016/j.tcb.2011.09.001

Weisenhorn, A. L., Drake, B., Prater, C. B., Gould, S. A., Hansma, P. K., Ohnesorge, F., Egger, M., Heyn, S. P. and Gaub, H. E. (1990). Immobilized proteins in buffer imaged at molecular resolution by atomic force microscopy. *Biophys. J.* **58**, 1251-1258. doi:10.1016/S0006-3495(90)82465-6

Xue, B., Leyrat, C., Grimes, J. M. and Robinson, R. C. (2014). Structural basis of thymosin-β4/profilin exchange leading to actin filament polymerization. *Proc. Natl. Acad. Sci. USA* **111**, E4596-E4605. doi:10.1073/pnas.1412271111

Yamashita, H., Taoka, A., Uchihashi, T., Asano, T., Ando, T. and Fukumori, Y. (2012). Single-molecule imaging on living bacterial cell surface by high-speed AFM. *J. Mol. Biol.* **422**, 300-309. doi:10.1016/j.jmb.2012.05.018

Yarar, D., Waterman-Storer, C. M. and Schmid, S. L. (2005). A dynamic actin cytoskeleton functions at multiple stages of clathrin-mediated endocytosis. *Mol. Biol. Cell* **16**, 964-975. doi:10.1091/mbc.e04-09-0774

Yokokawa, M., Wada, C., Ando, T., Sakai, N., Yagi, A., Yoshimura, S. H. and Takeyasu, K. (2006). Fast-scanning atomic force microscopy reveals the ATP/ADP-dependent conformational changes of GroEL. *EMBO J.* **25**, 4567-4576. doi:10.1038/sj.emboj.7601326

Yoshida, A., Sakai, N., Uekusa, Y., Deguchi, K., Gilmore, J. L., Kumeta, M., Ito, S. and Takeyasu, K. (2015). Probing in vivo dynamics of mitochondria and cortical actin networks using high–speed atomic force/fluorescence microscopy. *Genes Cells* **20**, 85-94. doi:10.1111/gtc.12204

Yoshida, A., Sakai, N., Uekusa, Y., Imaoka, Y., Itagaki, Y., Suzuki, Y. and Yoshimura, S. H. (2018). Morphological changes of plasma membrane and

protein assembly during clathrin-mediated endocytosis. *PLoS Biol.* **16**, e2004786. doi:10.1371/journal.pbio.2004786

Zhang, B., Koh, Y. H., Beckstead, R. B., Budnik, V., Ganetzky, B. and Bellen, H. J. (1998). Synaptic vesicle size and number are regulated by a clathrin adaptor protein required for endocytosis. *Neuron* **21**, 1465-1475. doi:10.1016/S0896-6273(00)80664-9

Zhang, Y., Yoshida, A., Sakai, N., Uekusa, Y., Kumeta, M. and Yoshimura, S. H. (2017). In vivo dynamics of the cortical actin network revealed by fast-scanning atomic force microscopy. *Microscopy* **66**, 272-282. doi:10.1093/jmicro/dfx015

Zhong, Q., Inniss, D., Kjoller, K. and Elings, V. B. (1993). Fractured polymer/silica fiber surface studied by tapping mode atomic force microscopy. *Surf. Sci. Lett.* **290**, L688-L692. doi:10.1016/0167-2584(93)90906-Y